Available online at www.sciencedirect.com
ScienceDirect
Journal of Nuclear Materials 374 (2008) 44–53
journal of nuclear materials
www.elsevier.com/locate/jnucmat

Modelling of grain face bubbles coalescence in irradiated UO_2 fuel

M.S. Veshchunov *

Nuclear Safety Institute (IBRAE), Russian Academy of Sciences, 52, B. Tulskaya, Moscow 115191, Russia

Received 27 October 2006; accepted 10 June 2007

Abstract

Two different mechanisms of grain face bubbles coalescence in irradiated UO_2 fuel are critically analysed and further developed. Coalescence of face bubbles due to their random migration is reconsidered on the base of the general theory for evolution of two-dimensional array of bubbles and shown to be effective for steady irradiation conditions and apparently insufficient for description of high-temperature annealing regimes. On the contrary, the improved mechanism of coalescence by growth and impingement of randomly distributed bubbles predicts rather weak decrease of face bubbles concentration under steady state irradiation conditions, however, becomes effective for simulation of high-temperature annealing tests with noticeable gas release. On this base, the general coalescence model which includes superposition of the two complementary mechanisms is formulated and proposed for implementation in the MFPR code.

1. Introduction

Kinetics of intergranular bubbles development is the key determination of the fission products release from irradiated UO_2 fuel and fuel pellets swelling. For this reason, many experimental investigations of bubbles growth and coalescence have been carried out, that allowed better understanding of these phenomena. However, there is still no general agreement what mechanisms are responsible for observed coalescence of intergranular bubbles during their growth under various conditions (steady irradiation, annealing or transient).

Zacharie et al. on the base of their tests [1] performed with pre-irradiated UO_2 fuel under high-temperature annealing conditions, assumed that during heat treatment grain face bubbles became mobile, migrated at random on grain surface and coalesced. Their model was later improved by Berdyshev and the author [2] (see also [3]) using the general theory of Krivoglaz [4] for bubbles coalescence by random migration on two-dimensional surfaces. However, in both models [1] and [2] the effective bubble mobility evaluated by fitting model calculations to measurements [1] turned to be several orders of magnitude higher in comparison with available data.

In a recent paper [5], White analysed an extensive set of experimental data on intergranular porosity development in various tests and proposed a new mechanism for intergranular bubbles coalescence based on consideration of the (immobile) nearest neighbours growth and overlapping in a random two-dimensional distribution of bubbles. This mechanism allowed a reasonable prediction of the critical grain face coverage of ≈19% at which the onset of bubble coalescence occurs, however, further progression of bubbles coalescence by the proposed mechanism was strongly overestimated.

The mechanism considered by White will be critically analysed and improved in the current paper, and then compared with the other coalescence mechanism proposed by Zacharie et al. [1]. It will be shown that depending on test conditions, each of these mechanisms can determine kinetics of intergranular bubbles coalescence during their growth and migration.

On the base of analysis of available experimental data, a new general model self-consistently considering both mechanisms will be finally formulated.

* Tel.: +7 495 955 2218; fax: +7 495 958 0040.
E-mail address: vms@ibrae.ac.ru

0022-3115/$ - see front matter © 2007 Elsevier B.V. All rights reserved.
doi:10.1016/j.jnucmat.2007.06.021

2. Coalescence by growth of randomly distributed bubbles

2.1. Model formulation

As proposed by White [5], the onset of the intergranular bubbles coalescence may be understood on the basis of a simple argument adapted to the two-dimensional case from the work of Chandrasekhar [6] who calculated the distribution of nearest neighbours in a random three-dimensional array of particles. For calculation of further bubbles progression, a more general kinetic model for the bubbles coalescence in the three-dimensional case with consideration of a real bubble size distribution function evolution developed by Mansur et al. [7,8], was adapted to the two-dimensional case in the mean-field approximation (with a mono-modal bubble size distribution function) [5].

Following this approach, it is assumed that fission gas atoms diffuse to the grain boundaries and are rapidly absorbed into the bubble nuclei randomly distributed over the surface. In the mean field approximation for the face bubbles with the mean circular projection radius $R(t)$ and the area $A = \pi R^2$, each bubble will be surrounded by a circle with the radius $2R$, in which no other bubble centres can reside. Any bubble centre located in this exclusion zone would find its perimeter within the perimeter of the parent bubble and coalescence would occur. Any further growth of the mean projected area of bubbles by an amount $\mathrm{d}A = 2\pi R\,\mathrm{d}R$, effectively increases the area of the exclusion zone by $4\,\mathrm{d}A$ and opens the possibility that $4N\,\mathrm{d}A$ bubbles may be swept out by the parent bubble.

In that event the bubble perimeters will interact and coalescence occurs. Considering each bubble in turn, the total rate of loss of bubbles by coalescence following an increase in area is given by:

$$\mathrm{d}N = -2N^2\,\mathrm{d}A,$$

or

$$\frac{\mathrm{d}N}{\mathrm{d}t} = -2N^2\frac{\mathrm{d}A}{\mathrm{d}t}, \tag{1}$$

where the factor of 4 is reduced to 2 to avoid counting each interaction twice.

The obtained in [5] Eq. (1) correctly describes a smooth growth of a bubble (by diffusion sinking of gas atoms) up to the moment of its coalescence with a neighbour, however, it does not take into consideration an abrupt jump of its size owing to coalescence. After averaging over distribution of bubbles, such jumps will disappear, however, effectively will enhance the mean bubble size growth rate.

In the mean field approximation such averaging procedure can be performed in the following way. At first, in the lack of the bubbles diffusion growth, one can notice that variation of the total occupied grain boundary area (coverage) due to bubbles coalescence (by any mechanism) is zero, $\mathrm{d}(N\overline{A})/\mathrm{d}t = 0$, where $\overline{A}$ is the bubbles averaged projection area. This reflects the mass conservation law for gas atoms (obeying the ideal gas state equation, if $R \geqslant 5$ nm) in equilibrium bubbles in the course of their coalescence (see Section 3.1). Therefore, the coverage can increase only owing to bubbles diffusion growth.

Indeed, in the case of non-zero bubbles diffusion growth, the mass conservation law takes the form

$$\frac{\mathrm{d}(N\overline{A})}{\mathrm{d}t} = N\frac{\partial\overline{A}}{\partial t}, \tag{2}$$

where

$$\frac{\mathrm{d}(N\overline{A})}{\mathrm{d}t} = N\frac{\mathrm{d}\overline{A}}{\mathrm{d}t} + \overline{A}\frac{\mathrm{d}N}{\mathrm{d}t}. \tag{3}$$

Here $\partial\overline{A}/\partial t$ denotes variation of the bubbles mean projection area owing solely to bubbles diffusion growth (considered in derivation of Eq. (1)), whereas $\mathrm{d}\overline{A}/\mathrm{d}t$ denotes total variation of the bubble mean area owing to bubbles growth and coalescence. In this new notation Eq. (1) takes the form

$$\frac{\mathrm{d}N}{\mathrm{d}t} = -2N^2\frac{\partial\overline{A}}{\partial t}. \tag{4}$$

Substituting Eqs. (2) and (4) in Eq. (3), one obtains

$$\frac{\mathrm{d}\overline{A}}{\mathrm{d}t} = (1 + 2N\overline{A})\frac{\partial\overline{A}}{\partial t}. \tag{5}$$

Superposition of Eqs. (4) and (5) yields

$$\frac{\mathrm{d}N}{\mathrm{d}\overline{A}} = -\frac{2N^2}{1 + 2N\overline{A}}. \tag{6}$$

This consideration is not valid at high coverage $S = N\overline{A}$, when probability of multiple coalescence among three and more bubbles becomes non-negligible leading to formation of interconnected bubbles chains. It is conventionally assumed that the onset of gas release through bubble interconnection commences after attainment of the saturation value $S^* \approx 0.5$. After this the total amount of gas atoms in the bubbles is not anymore conserved, so, Eq. (2) is not anymore valid. In this stage the bubbles coalescence obeys the saturation coverage condition

$$N\overline{A} = 0.5, \tag{7}$$

or

$$\frac{\mathrm{d}(N\overline{A})}{\mathrm{d}t} = N\frac{\mathrm{d}\overline{A}}{\mathrm{d}t} + \overline{A}\frac{\mathrm{d}N}{\mathrm{d}t} = 0, \tag{7'}$$

instead of Eq. (6), since the diffusion flux $J_{\mathrm{dif}}(t)$ flux from the grain bulk to the grain boundaries is completely transferred into open porosity via interconnected face bubbles (see Section 4).

2.2. Model solution

An explicit solution of Eq. (6) can be searched in the following way. Substitution of Eq. (5) into Eq. (2) yields

$$\frac{\mathrm{d}(N\overline{A})}{\mathrm{d}t} = \frac{N}{1 + 2N\overline{A}}\frac{\mathrm{d}\overline{A}}{\mathrm{d}t},$$

or

$$\frac{\mathrm{d}(N\overline{A})}{\mathrm{d}\overline{A}} = \frac{N}{1+2N\overline{A}} = \frac{1}{\overline{A}}\frac{N\overline{A}}{1+2N\overline{A}},$$

or

$$\frac{\mathrm{d}(N\overline{A})}{\mathrm{d}(\ln\overline{A})} = \frac{N\overline{A}}{1+2N\overline{A}}. \tag{8}$$

Solution of Eq. (8) has the form

$$N\overline{A} = N_0\overline{A}_0 + \frac{1}{2}\ln\frac{N_0}{N}, \tag{9}$$

or

$$N = N_0\exp\left(-2\left(N\overline{A} - N_0\overline{A}_0\right)\right). \tag{10}$$

This implies that variation of N_0/N is much slower than predicted by Eq. (1). Indeed, analysis of Eq. (10) shows that in the case $N_0\overline{A}_0 \to 0$, N_0/N varies from 1 (when $N\overline{A} = N_0\overline{A}_0$) to $e^2 \approx 7.4$ (when formally $N\overline{A} \to 1$); the saturation value $N\overline{A} = 0.5$ is attained at $N_0/N = e \approx 2.7$, whereas Eq. (1) erroneously predicts variation of N_0/N within several orders of magnitude, as shown in Fig. 6 of [5].

Therefore, coalescence by the proposed mechanism is not strong and provides only ≈3-fold reduction of the bubbles surface concentration before attainment of the saturation coverage. In this situation, an enhanced face bubbles coalescence observed under normal irradiation conditions [9] and characterised by 1–2 orders of magnitude reduction of N, may be explained by another mechanism considered in Section 3.

On the other hand, as above explained, after attainment of the saturation coverage ≈0.5, Eq. (9) is not anymore valid. During the saturation stage the variation of N becomes significantly steeper, as seen from Eq. (7)

$$N = 0.5\overline{A}^{-1}. \tag{11}$$

This case will be considered in Section 4.

3. Bubbles coalescence by random migration

3.1. Model formulation

In order to explain the observed kinetics of grain face swelling under annealing conditions, Zacharie et al. [1] assumed that during heat treatment face bubbles became mobile and migrated at random on grain surface, and then coalesced. The theory of coalescence of bubbles in a two-dimensional array based on the analysis of the bubble size distribution function evolution was developed by Krivoglaz [4]. Apparently lacking these theoretical results, the authors [1] attempted their own approach to the same problem. Despite that their new calculations were rather cumbersome, Zacharie et al. managed to reproduce the main kinetic dependencies of bubble concentration and size on time in a qualitative agreement with the general theory [4]. As a result, an explicit equation for intergranular swelling as a function of treatment time and temperature was derived in their work. This equation provided a good description of the measured swelling values after fitting of the main model parameter (bubble diffusivity).

In the subsequent paper of Berdyshev and the author [2] the general theory [4] for the bubbles coalescence kinetics was adapted to the two-dimensional case in the mean-field approximation (with a mono-modal bubble size distribution function), and the main analytical results of [1] were deduced in a more straightforward and simple way (see also [3]). This allowed elimination of some inconsistencies in the approach of [1] and improvement of the model predictions.

However, in both models [1] and [2] the effective bubble diffusivity evaluated by fitting of the model predictions to the experimental data [1] turned to be several orders of magnitude higher in comparison with the conventional data for the bubble diffusivity.

Indeed, the diffusion coefficient D_b determined by the surface diffusion mechanism (apparently the most rapid and thus rate determining for UO_2) of spherical intragranular bubble migration was evaluated by Shewmon [10] as $D_\mathrm{b} = 3D_\mathrm{s}\Omega^{4/3}/2\pi R_\mathrm{b}^4$, where D_s is the surface self-diffusion coefficient, R_b is the bubble radius, $\Omega \approx 4.1\times10^{-29}\,\mathrm{m}^3$ is the atomic volume. For lenticular grain face bubbles with the semi-dihedral angle $\theta \approx 50°$ and the projection radius $\rho_\mathrm{b} = R_\mathrm{b}\sin\theta$ the bubble diffusivity depends on the migration direction. In the case of migration in the direction of the grain boundary relocation (perpendicular to the grain boundary), the bubble diffusivity was recently calculated by the author as $D_\mathrm{b} = \left(3D_\mathrm{s}\Omega^{4/3}/2\pi\rho_\mathrm{b}^4\right)\cdot\sin^4\theta/(1-\cos^3\theta) \approx 3D_\mathrm{s}\Omega^{4/3}/4\pi\rho_\mathrm{b}^4$ [11]. A similar calculation for bubble migration along the surface of the grain boundary yields

$$D_\mathrm{b} = \frac{3D_\mathrm{s}\Omega^{4/3}}{2\pi\rho_\mathrm{b}^4}\sin\theta \approx 0.77\cdot\frac{3D_\mathrm{s}\Omega^{4/3}}{2\pi\rho_\mathrm{b}^4}. \tag{12}$$

The data for the surface diffusion coefficient obtained by mass transfer methods give the following relationship for the surface diffusion coefficient of uranium atoms [12]:

$$D_\mathrm{s}[\mathrm{m}^2/\mathrm{s}] = 50\cdot\exp(-450\,000/RT), \tag{13}$$

with $1473 < T < 2073$ K and R in J mol^{-1} K^{-1}.

Despite the values of D_s from Eq. (13) have been estimated by Matzke [13] to be within an experimental scatter band of two orders of magnitude for the temperature range examined, they provided a very low mobility (by several orders of magnitude) of face bubbles in comparison with the mobility necessary for correct description of Zacharie's observations [1] by the proposed random migration mechanism (see [3]).

On the other hand, results of the tracer studies of Marlowe and Kazanoff [14] corrected by Olander [15] were confirmed by Zhou and Olander [16] giving much higher values for the surface diffusion coefficient D_s (e.g., five orders of magnitude higher than predicted by Eq. (13) at 1988 K)

with a pre-exponential coefficient of $D_0 \sim 5\times10^2$ m^2/s and an activation energy of 300 ± 60 kJ/mol. The latter value is in a rather good agreement with the value of 310 kJ/mol obtained by Zacharie et al. [1] for the activation energy of random migration of grain face bubbles. This value of the activation energy was also used in fitting calculations [2,3] with the pre-exponential coefficient of $D_0 \sim 10^2$ m^2/s, however, with a somewhat slower dependence of the bubble diffusivity from the bubble projection radius, $\propto \rho_b^{-3.4}$, which is avoided in the current model formulation, Eq. (12).

For this reason, it is attempted to use for the surface diffusion coefficient D_s the following Arrhenius correlation, based on the evaluation [16] and consistent with the activation energy measurements in [1]:

$$D_s[\mathrm{m}^2/\mathrm{s}] = D_0\cdot\exp\left(-\frac{Q}{RT}\right) = 5\cdot10^2\exp\left(-\frac{310000}{RT}\right) = 5\cdot10^2\exp\left(-\frac{37286.5}{T}\right). \quad (14)$$

Nevertheless, one should keep in mind that the surface diffusivity from Eq. (14) is extremely high, e.g., at 1988 K $D_s \approx 3.6\times10^{-6}$ m^2/s is comparable with the gaseous Xe self-diffusivity; therefore, rather exotic mechanisms have to be engaged to ground this option [15,16]. Furthermore, mobility of small bubbles (with radius up to 10 nm) in UO_2 directly measured in various tests [17–19] is suitably described by the surface diffusion mechanism with the standard surface diffusivity from Eq. (13) [20], being therefore in remarkable contradiction with Eq. (14).

In the mean field approximation (considering only the mean bubble size) variation of the surface concentration of face bubbles N due to coalescence obeys the rate equation [2,3]

$$\frac{\mathrm{d}N}{\mathrm{d}t} = -\omega_{\mathrm{cls}}N^2. \quad (15)$$

The coalescence frequency of bubbles randomly moving on a surface can be represented by the formula derived in [4]

$$\omega_{\mathrm{cls}} = \frac{8\pi D_b}{\ln\left(D_b\tau_0/2\rho_b^2\right)} \approx 8\pi\alpha D_b, \quad (16)$$

which is valid with the logarithmic accuracy under condition $|\ln S| \gg 1$, where $S = AN = \rho_b^2/R_c^2$ is the surface coverage, $R_c \approx (\pi N)^{-1/2}$ is the radius of the bubble sinking zone, τ_0 is the characteristic time of the two-fold increase of the mean bubble projection radius ρ_b, evaluated as $\tau_0 \approx R_c^2/D_b$. Being a weak (logarithmic) function of its argument, the parameter $\alpha \approx |\ln S|^{-1}$ slowly varies from 0.15 to 0.4 at low coverage (from 0.001 to 0.1) and will be approximated by a constant value ≈0.2.

At first, the simplest case with invariable grain face coverage is considered

$$N\overline{A} = N\pi\rho_b^2 = \mathrm{const} = N_0\pi\rho_0^2 = N_0\overline{A}_0, \quad (17)$$

where N_0 and ρ_0 are the initial concentration and mean projection radius of bubbles at the moment t_0, respectively. For instance, this case is realised in the lack of the diffusion flux from the grain bulk to the grain boundaries.

A more realistic realisation of Eq. (17) appears after attainment of the saturation coverage $S^* \approx 0.5$, when the diffusion flux is completely compensated by the release flux into open porosity; however, in this case the condition $|\ln S| \approx \alpha^{-1} \gg 1$ of applicability of Eq. (16) is not valid. This implies, in particular, that formal extension of the model to consideration of high-temperature annealing tests (in which the saturation coverage is sustained) is not completely reliable. Nevertheless, it will attempted below (in Section 3.2), in order to consider this situation approximately.

The system of Eqs. (12) and (15)–(17) results in the equation

$$\frac{\mathrm{d}N}{N^4} = -\frac{12\alpha D_s\Omega^{4/3}\sin\theta}{N_0^2\rho_0^4}\mathrm{d}t \approx -\frac{9\alpha D_s\Omega^{4/3}}{N_0^2\rho_0^4}\mathrm{d}t, \quad (18)$$

which has the solution

$$\frac{N_0^3}{N^3} = 1 + \frac{27\alpha D_s\Omega^{4/3}N_0}{\rho_0^4}(t-t_0). \quad (19)$$

This solution (valid under simplifying condition, Eq. (17)) corresponds to the considerations in the previous papers [1–3].

In a more general case, when the saturation coverage is not attained, Eq. (17) should be substituted by the mass balance equation

$$\frac{\mathrm{d}(N\cdot N_g)}{\mathrm{d}t} = 2J_{\mathrm{dif}}, \quad (20)$$

where $J_{\mathrm{dif}}(t)$ is the diffusion flux to a grain boundary from each of two neighbouring grains, N_g is the mean number of gas atoms in a face bubble. In neglect of the external pressure in comparison with the internal bubble pressure, it obeys the ideal gas state law (if approximately $\rho_b \geqslant 5$ nm)

$$N_g = \frac{P_bV_b}{kT} = \frac{8\pi\gamma\rho_b^2}{3kT}\varphi(\theta), \quad (21)$$

where $\varphi(\theta) = (1 - 1.5\cos\theta + 0.5\cos^3\theta)\sin^{-2}\theta \approx 0.29$ for lenticular bubbles, $\gamma \approx 1$ J/m^2 is the surface tension [21].

Therefore, integrating Eq. (20) one obtains

$$N\rho_b^2 = N_0\rho_0^2 + f(t), \quad (22)$$

where

$$f(t) = \frac{3kT}{4\pi\gamma\varphi(\theta)}\int_{t_0}^{t} J_{\mathrm{dif}}(t)\mathrm{d}t,$$

or, in accordance with Eq. (2)

$$N\frac{\partial\overline{A}}{\partial t} = \frac{3kT}{4\gamma\varphi(\theta)}J_{\mathrm{dif}}(t) \quad (23)$$

After substitution of Eq. (22) in Eq. (15) one obtains the equation

$$\frac{dN}{N^4} = -\frac{9\alpha D_s \Omega^{4/3}}{N_0^2 \rho_0^4}\left(1+\frac{f(t)}{N_0\rho_0^2}\right)^{-2} dt, \quad (24)$$

which has the solution

$$\frac{N_0^3}{N^3} = 1 + \frac{27\alpha D_s N_0 \Omega^{4/3}}{\rho_0^4}\int_{t_0}^{t}\left(1+\frac{f(t)}{N_0\rho_0^2}\right)^{-2} dt. \quad (25)$$

3.2. Analysis of experiments

Microscopic behaviour of intergranular bubbles under steady irradiation conditions was observed by Kashibe and Une [9]. The specimens were taken from UO_2 pellets irradiated in commercial BWR (burn-up: 6–28 GW d t^{-1}) at a point between the fuel rim and middle. Grain face bubble concentration and fractional coverage were examined by scanning electron microscope fractography. In addition, radii of face bubbles were also evaluated. The irradiation temperature at the location of the specimens may be evaluated as ~1500 K from their maximum linear heat generation rates (between 300 and 370 W/cm). The grain sizes of the fuel and irradiation rate were approximately equal to 9 μm and 1.8×10^{19} m^{-3} s^{-1}, respectively. During irradiation the concentration of the intergranular bubbles at first increased owing to bubbles nucleation from $\sim1.6\times10^{13}$ m^{-2} (at burn-up ~16 GW d t^{-1}) to $\sim4\times10^{13}$ m^{-2} (at burn-up ~23 GW d t^{-1}) and then dropped to $\sim1.6\times10^{12}$ m^{-2} (at burn-up ~28 GW d t^{-1}). The mean bubble projection radius increased from ~20 nm at 23 GW d t^{-1} to ~110 nm at 28 GW d t^{-1}, and fractional coverage correspondingly increased from ~5% to ~10%. Therefore, one can conclude that the bubbles coalescence prevailed over generation of new bubbles on grain faces in the late stage of irradiation (from 23 to 28 GW d t^{-1}). This is in a qualitative agreement with the assumption of White [5] that, once coalescence of face bubbles occurs, the geometric size of the initial population would tend to absorb any newly nucleated bubbles giving the effect that the nucleation was a one-off process.

In order to simulate the bubbles coalescence during irradiation period between 23 and 28 GW d t^{-1}, the following parameters of Eq. (22) are chosen in accordance with the above presented experimental data:

$t_0 \approx 6\cdot10^7$ s, $t_f \approx 7\cdot10^7$ s and

$f(t_f) \approx N_0\rho_0^2$, since $N(t_f)\rho_b^2(t_f) \approx 2N_0\rho_0^2$.

Owing to monotonic growth of the function $f(t)$, one can evaluate for this case

$$\frac{\Delta t}{4} < \int_{t_0}^{t_f}\left(1+\frac{f(t)}{N_0\rho_0^2}\right)^{-2} dt < \Delta t, \quad (26)$$

where $\Delta t = t_f - t_0$. Therefore, from Eq. (25) one obtains

$$1 + \frac{27\alpha D_s \Omega^{4/3} N_0}{4\rho_0^4}\Delta t < \frac{N_0^3}{N^3} < 1 + \frac{27\alpha D_s \Omega^{4/3} N_0}{\rho_0^4}\Delta t, \quad (27)$$

or

$$\left(1+\frac{27\alpha D_s \Omega^{4/3} N_0}{4\rho_0^4}\Delta t\right)^{1/3} < \frac{N_0}{N} < \left(1+\frac{27\alpha D_s \Omega^{4/3} N_0}{\rho_0^4}\Delta t\right)^{1/3}. \quad (28)$$

For the test conditions ($T\approx1500$ K, $N_0\approx4\times10^{13}$ m^{-2}), Eqs. (28) and (14) yields $60 < N_0/N < 10^2$, or 4×10^{11} $m^{-2} < N < 6\times10^{11}$ m^{-2}, in a reasonable agreement with the measured value $N\approx1.6\times10^{12}$ m^{-2}. Some underestimation of the final concentration might be connected with unaccounted new bubbles generation during the considered period, and/or with the above discussed uncertainty of the used correlation for the surface diffusivity, Eq. (14), as well as uncertainty in evaluation of the parameter α in Eq. (16).

Therefore, one can conclude that the coalescence mechanism might be effective in the steady irradiation tests [9], in which face bubbles were relatively small, $\rho_0 \leqslant 0.1$ μm.

However, under high-temperature annealing conditions when the mean bubble radius rapidly increases during heat-up stage and exceeds 0.1 μm, the bubbles mobility ($\propto \rho_b^{-4}$) decreases making this coalescence mechanism less effective.

Indeed, for the annealing tests [1] (described in more detail in the next Section 4) the model for bubbles coalescence by their random migration apparently underpredicts the coalescence rates measured at temperatures 1683–1988 K, even if the same correlation, Eq. (14), which provides a reasonable agreement with the steady irradiation tests, is used.

At high-temperature 1988 K in the period from the initial moment $t_0 = 3\times10^2$ s to the final moment $t_f = 3.6\times10^4$ s the mean projected bubble radius increased from ~0.3 μm to ~0.7 μm and the surface concentration of bubbles N decreased from $\sim1.7\times10^{12}$ m^{-2} to $\sim0.34\times10^{12}$ m^{-2}, the coverage being fairly constant ≈0.49–0.55 and rather close to the theoretical value of the saturation coverage 0.5. Application of Eq. (19) to the annealing test conditions results in a notable underestimation of the bubble coalescence, $N_0/N \approx 1.46$ and $\rho_b/\rho_0 \approx 1.21$, in comparison with the experimentally measured values ≈5 and 2.3, respectively.

The agreement with the measurements can be somewhat improved by formal extension of the parameter $\alpha \approx |\ln S|^{-1}$ (which should be $\ll1$) from 0.2 (corresponding to low coverages) to 1. The best fit to experimental data can be obtained, however, only by multiplication of the surface diffusivity, Eq. (14), by an additional factor of 50 Fig. 1. This apparently brings the surface diffusivity value out of the physically grounded limits (see remarks presented after Eq. (14)).

The model underestimation is also strong at lower temperatures, e.g. during annealing at 1818 K from $t_0 = 1.8\times10^3$ s to $t_f = 3.6\times10^4$ s (at almost constant coverage

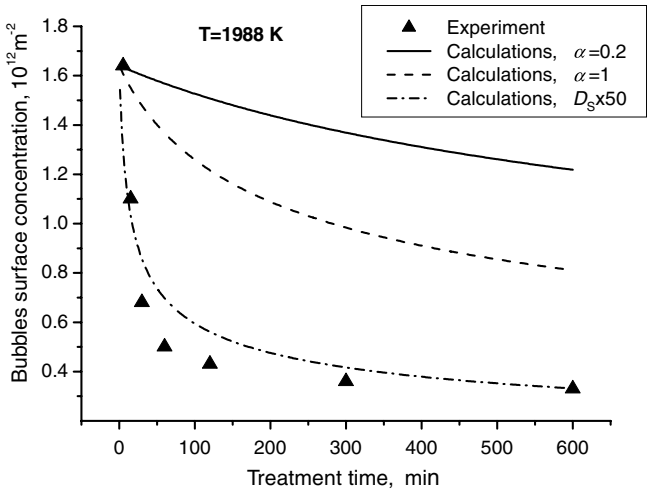

Fig. 1. Variation of the bubbles surface concentration with the treatment time at the annealing temperature 1988 K in the tests [1]. Comparison of measurements with calculations using the random migration mechanism for bubbles coalescence with two values of the model parameter $\alpha = 0.2$ and 1, and with the surface diffusivity increased by a factor of 50.

0.48–0.56) the calculated values are $N_0/N \approx 1.2$ and $\rho_b/\rho_0 \approx 1.1$, whereas the experimentally measured values were ≈2.6 and 1.6, respectively. Similarly to the case of 1988 K, the best fit is attained only by multiplication of the surface diffusivity by a factor of 30 Fig. 2.

It is clear that application of a more widely used correlation for the surface diffusion coefficient, Eq. (13), instead of Eq. (14) will completely suppress the bubbles coalescence rate.

Therefore, the other coalescence mechanism by growth of randomly distributed bubbles (presented in Section 2) will be reconsidered for annealing conditions as a complementary approach. As mentioned in Section 2, being rather weak at low coverage, this mechanism becomes much more effective after attainment of the saturation coverage that is typical for the annealing conditions.

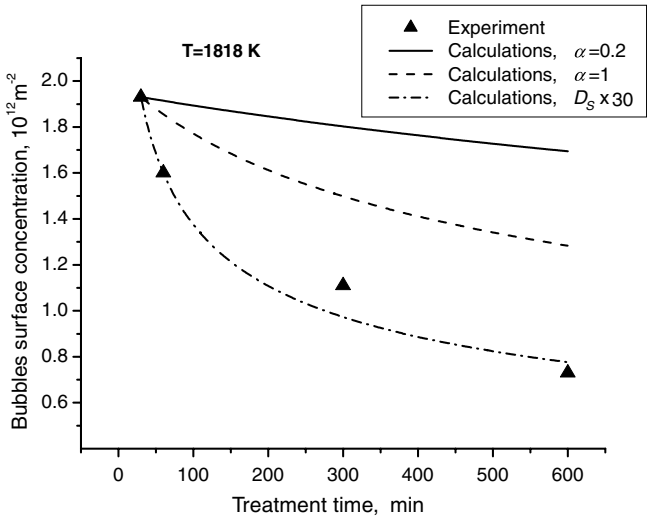

Fig. 2. Variation of the bubbles surface concentration with the treatment time at the annealing temperature 1818 K in the tests [1]. Comparison of measurements with calculations using the random migration mechanism for bubbles coalescence with two values of the model parameter $\alpha = 0.2$ and 1, and with the surface diffusivity increased by a factor of 30.

4. Bubbles coalescence at the saturation coverage

4.1. Model formulation

As above mentioned, consideration of the grain face bubbles coalescence mechanism presented in Section 2 is valid until coverage attains the saturation value ≈0.5, i.e. $N\overline{A} \leqslant 0.5$. In accordance with the percolation mechanism [22], after attainment of the saturation coverage manifested by face bubbles interlinkage and formation of channels (or bubble chains) on grain faces interconnected with open porosity (at grain edges), gas release (venting) from face bubbles through the channels commences.

Owing to gas venting (with the flux denoted as $J_{out}(t)$), the chains collapse and disintegrate in a smaller amount of bubbles diminishing the mean surface concentration of bubbles with a rate denoted as $\partial N/\partial t$, thus reducing the grain face coverage (proportional to total amount of gas atoms in bubbles) below the saturation value.

Since face bubbles continue to grow owing to the diffusion flux from the grain bulk $2J_{dif}(t)$, the saturation coverage and bubbles interlinkage quickly reinstate and the processes of gas venting and bubble chains collapse repeat, and so on, keeping the mean coverage close to the saturation value, while the mean bubble size $\overline{A}(t)$ continuously increases (however, with a decreased rate).

In this case, instead of Eq. (2), which is not anymore valid because of gas venting, the mass balance equation in the mean field approximation takes the form

$$\frac{d(N\overline{A})}{dt} = N\frac{\partial \overline{A}}{\partial t} + \overline{A}\frac{\partial N}{\partial t}, \tag{29}$$

and, instead of Eq. (23)

$$N\frac{\partial \overline{A}}{\partial t} + \overline{A}\frac{\partial N}{\partial t} = \frac{3kT}{8\gamma\varphi(\theta)}(2J_{dif} - J_{out}), \tag{29'}$$

where, as before, $\partial\overline{A}/\partial t$ denotes the bubbles diffusion growth rate and $\partial N/\partial t$ denotes variation of the bubbles surface concentration owing to chains collapse (as above described).

In the simplest approach one can assume that the venting flux $J_{out}(t)$ is completely balanced by the rate of bubbles vanishing in the process of chains collapse, i.e. $J_{out} = -(3kT/8\gamma\varphi(\theta))^{-1}\overline{A}\partial N/\partial t$. In this case, as results from Eq. (29), the diffusion growth of the bubble mean size is not violated and obeys Eq. (23) as before. However, as will be shown below, in this case the model significantly overestimates the bubbles coalescence rate.

More generally one should assume that only some part $\beta \leqslant 1$ of the release flux corresponds to bubble vanishing, i.e. $\beta J_{out} = -(3kT/8\gamma\varphi(\theta))^{-1}\overline{A}\partial N/\partial t$, whereas the other part $(1-\beta)$ of the flux reduces the size of non-vanished

bubbles in the chains. In this case the diffusion growth rate of the bubble mean size is also violated, i.e. $(3kT/8\gamma\varphi(\theta))^{-1}N\partial\overline{A}/\partial t = 2J_{\rm dif} - (1-\beta)J_{\rm out}$, as can be deduced from Eq. (29′).

On the other hand, in this stage bubbles coalescence additionally obeys the saturation coverage condition

$$N\overline{A} = 0.5, \tag{30}$$

or

$$\frac{{\rm d}(N\overline{A})}{{\rm d}t} = N\frac{{\rm d}\overline{A}}{{\rm d}t} + \overline{A}\frac{{\rm d}N}{{\rm d}t} = 0. \tag{30′}$$

Under condition of the invariable coverage, Eq. (30′), corresponding to conservation of the total amount of gas atoms in grain face bubbles (see Section 3.1), the diffusion flux $2J_{\rm dif}(t)$ to the grain boundaries is completely transferred into open porosity via interconnected face bubbles and thus is compensated by the release flux $J_{\rm out}(t)$, i.e. $2J_{\rm dif}(t) = J_{\rm out}(t)$. Therefore, the mass balance equation, Eq. (29), can be represented in the form:

$$\frac{{\rm d}(N\overline{A})}{{\rm d}t} = N\frac{\partial\overline{A}}{\partial t} - \beta\frac{3kT}{4\gamma\varphi(\theta)}J_{\rm dif}(t) = 0, \tag{31}$$

instead of Eq. (23). The model parameter β effectively describes in the mean-field approximation a rather complicated process of gas venting and for this reason cannot be determined mechanistically in the current approach. Therefore, it will be determined below by fitting the model calculations to the experimental data.

The coalescence rate equation, Eq. (4), based on consideration of the couple coalescence with the nearest neighbours, at saturation coverage should be supplemented with an additional term describing the bubbles coalescence rate owing to channels formation and collapse, denoted above as $\partial N/\partial t$

$$\frac{{\rm d}N}{{\rm d}t} = -2N^2\frac{\partial\overline{A}}{\partial t} + \frac{\partial N}{\partial t}. \tag{32}$$

The system of equations, Eqs. (29)–(32), completely determines the evolution of face bubbles during coalescence at the critical coverage. Indeed, superposition of Eqs. (29), (30′) and (32) yields

$$\frac{{\rm d}\overline{A}}{{\rm d}t} = (1+2N\overline{A})\frac{\partial\overline{A}}{\partial t} = 2\frac{\partial\overline{A}}{\partial t}, \tag{33}$$

and taking into account from Eqs. (30) and (30′) that:

$$\frac{{\rm d}N}{{\rm d}t} = -2N^2\frac{{\rm d}\overline{A}}{{\rm d}t}, \tag{34}$$

one obtains a relationship

$$\frac{{\rm d}N}{{\rm d}t} = -4N^2\frac{\partial\overline{A}}{\partial t}. \tag{35}$$

Substitution of Eq. (31) in Eq. (35) finally results in a new coalescence rate equation

$$\frac{{\rm d}N}{N} = -\frac{3\beta kT}{\gamma\varphi(\theta)}J_{\rm dif}(t){\rm d}t, \tag{36}$$

which has the solution

$$\ln\left(\frac{N}{N_0}\right) = -\frac{3\beta kT}{\gamma\varphi(\theta)}\int_{t_0}^{t}J_{\rm dif}(t){\rm d}t = -\frac{3\beta kT}{\gamma\varphi(\theta)}F(t), \tag{37}$$

where

$$F(t) = \int_{t_0}^{t}J_{\rm dif}(t){\rm d}t,$$

or

$$\frac{N}{N_0} = \exp(-4\pi\beta f(t)) = \frac{\overline{A}_0}{\overline{A}}, \tag{38}$$

where $f(t) = (3kT/4\pi\gamma\varphi(\theta))F(t) = (3kT/4\pi\gamma\varphi(\theta))\int_{t_0}^{t}J_{\rm dif}(t){\rm d}t$.

Therefore, the concentration variation is characterised by a rather strong (exponential) dependence on gas release and thus can be significant under heat-up conditions of high-temperature annealing or transient tests.

4.2. Analysis of experiments

Detailed experimental study of the bubble growth and coalescence kinetics under annealing conditions was carried out in [1]. In these tests the intergranular swelling for similar base-irradiated samples, was measured at various annealing times along with observations of the grain face microstructure evolution. Unstressed samples of uranium dioxide taken from the pressurised water reactor fuel after two normal operating cycles, i.e., with burn-up of ~25 GW d/t U, were subjected to thermal treatment in a laboratory furnace at temperatures between 1403 and 1988 K for duration between 5 min and 10 h. During irradiation stage fuel core temperature did not exceed 1373 K. The variation of the quantity of fission gas released over time was measured at each temperature. The samples were also subjected to a series of isothermal swelling measurements. Their comparison provides information on the intergranular, intragranular, open and closed porosity.

It is straightforward to evaluate from the test data that the saturation coverage ≈0.5 was attained very quickly, at least after 3×10^2 s at 1988 K, and then kept fairly constant. As indicated in Section 3.2, at high-temperature 1988 K in the period from the initial moment $t_0 = 3\times10^2$ s to the final moment $t_f = 3.6\times10^4$ s the mean bubble projection radius $\rho_{\rm b}$ increased from ~0.32 to ~0.7 μm and the surface concentration of bubbles N reduced from $\sim1.7\times10^{12}$ m^{-2} to $\sim0.34\times10^{12}$ m^{-2}. During this period gas release, which is proportional to $F(t)$ (defined in Eq. (37)), varied from ≈10 to ≈30% and thus made up ≈20%. Taking into account that the fuel burn-up was estimated in [1] as 25 GW d t^{-1} equivalent to the total fission gas atoms generation $\approx1.6\times10^{26}$ m^{-3}, and the mean grain diameter as 9.3 μm, one can evaluate that $F(t)$ attained $\approx0.5\times10^{20}$ m^{-2} in this test. Substituting these values in

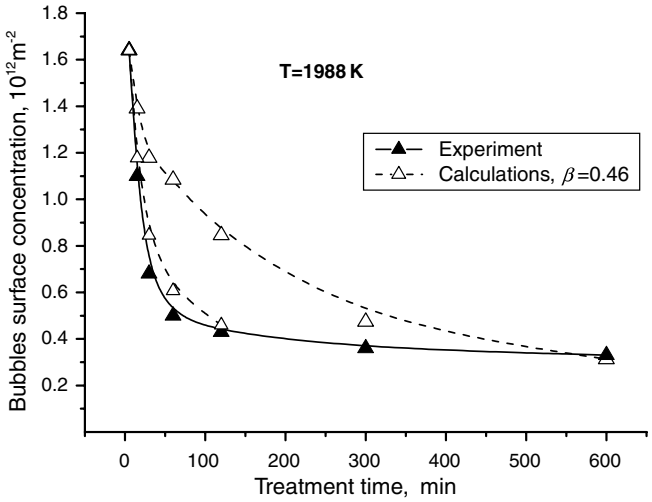

Fig. 3. Variation of the bubbles surface concentration with the treatment time at the annealing temperature 1988 K in the tests [1]. Comparison of calculations using the coalescence mechanism by growth of randomly distributed bubbles with the model parameter $\beta = 0.46$ against two sets of experimental data for gas release during coalescence at the critical coverage.

Eq. (38) and using the maximum value of the model parameter $\beta = 1$, one can find that at $t_f = 3.6 \times 10^4$ s reduction of the bubbles concentration is overestimated by one order of magnitude ($N_0/N \approx 36$ instead of ≈ 5). To avoid this strong overestimation, one should choose a smaller value of $\beta \approx 0.46$, see Fig. 3.

At lower temperatures the agreement is also reasonable, for instance, at 1818 K in the interval from $t_0 = 3 \times 10^3$ s (when the coverage attained the saturation value) to $t_f = 3.6 \times 10^4$ s gas release was $\approx 6\%$, therefore, $F(t)$ attained $\approx 0.15 \times 10^{20}$ m^{-2} in this test. In this case Eq. (38) with the same parameter $\beta = 0.46$ predicts decrease of the concentration $N_0/N \approx 1.6$ and increase of the mean

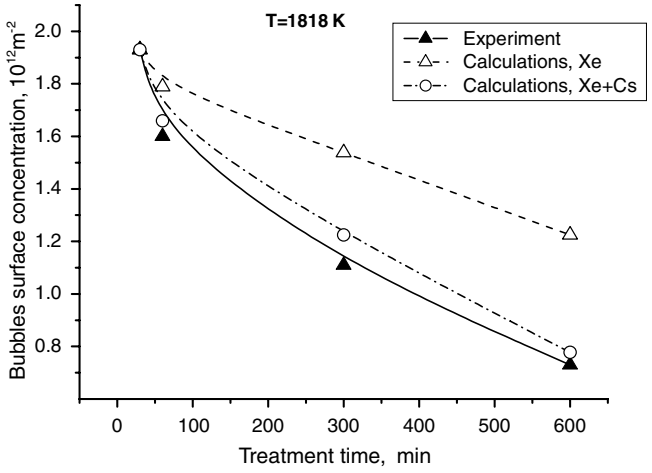

Fig. 4. Variation of the bubbles surface concentration with the treatment time at the annealing temperature 1818 K in the tests [1]. Comparison of measurements with calculations using the coalescence mechanism by growth of randomly distributed bubbles ($\beta = 0.46$) with and without consideration of Cs release during coalescence at the critical coverage.

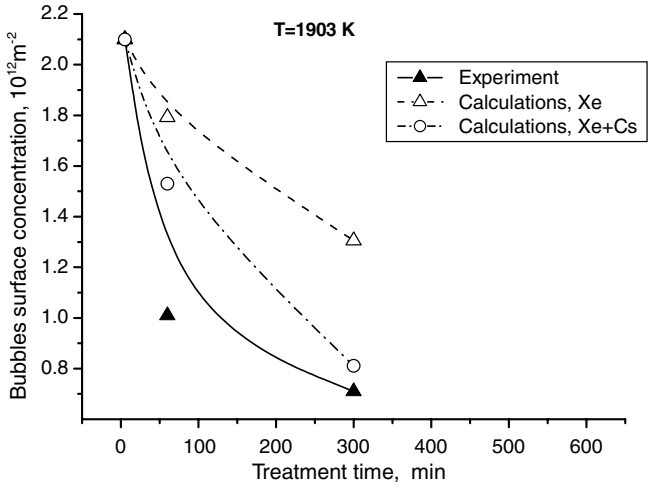

Fig. 5. Variation of the bubbles surface concentration with the treatment time at the annealing temperature 1903 K in the tests [1]. Comparison of measurements with calculations using the coalescence mechanism by growth of randomly distributed bubbles ($\beta = 0.46$) with and without consideration of Cs release during coalescence at the critical coverage.

bubble projection radius $\rho_b/\rho_0 \approx 1.3$, whereas the measured values were ≈ 2.6 and 1.6, respectively Fig. 4.

Further improvement of the model predictions can be obtained by additional consideration of evaporation of chemically active elements (mainly Cs) into bubbles at grain faces that can notably enhance the source term $J_{out}(t) = 2J_{dif}(t)$ at annealing temperatures (by adding the evaporation flux $J_{evap}(t)$, i.e. $2J_{dif}(t) \rightarrow 2J_{dif}(t) + J_{evap}(t)$) and thus increase $F(t)$ in Eqs. (37) and (38), resulting in the enhancement of the bubbles coalescence rate. This is illustrated in Fig. 4 by the second (dashed) calculated curve, where it is assumed $J_{evap}(t) \approx J_{out}(t)$, since normally in the annealing tests the Cs release is comparable with the gas release.

This model improvement (along with the final fitting of the parameter β) can be realised by adequate calculation of Cs release after implementation of the model in the MFPR code [3] designed for mechanistic calculation of fission products (FP) release with self-consistent consideration of FP chemical interactions and fuel microstructure evolution (see Section 5).

At temperature 1903 K a similar release ≈ 5–6% occurred during a shorter annealing period from 3×10^2 to 1.8×10^4 s. During this period variation of concentration predicted by the model with and without consideration of evaporation flux shows the same tendency as at 1818 K, see Fig. 5.

At the lowest test temperature 1683 K the concentration was measured only at two moments and the saturation coverage was not attained in the first measurement point ($S \leqslant 0.4$); for this reason, calculation of this test was not attempted.

5. General formulation of the coalescence model

In the general case one should consider superposition of the two coalescence mechanisms by random bubbles

migration and by bubbles growth. In this case probability of a bubble coalescence with its neighbours during time interval dt is the sum of probabilities of two independent events described by Eqs. (4) and (15), respectively. Therefore, the bubbles coalescence rate at low coverage in the mean field approximation takes the form:

$$\frac{dN}{dt} = -2N^2\frac{\partial\overline{A}}{\partial t} - \omega_{cls}N^2. \tag{39}$$

Substitution of Eqs. (23) and (24) in Eq. (39) yields

$$\frac{dN}{dt} = -N\frac{3kT}{2\gamma\varphi(\theta)}J_{dif}(t) - N^4\frac{9\pi^2\alpha D_s\Omega^{4/3}}{N_0^2\overline{A}_0^2}\left(1+\frac{\pi f(t)}{N_0\overline{A}_0}\right)^{-2}, \quad \text{if } N\overline{A} < 0.5. \tag{40}$$

At the saturation coverage Eq. (39) should be supplemented with the additional term describing the bubbles coalescence rate owing to channels formation and collapse from Eq. (32)

$$\frac{dN}{dt} = -2N^2\frac{\partial\overline{A}}{\partial t} - \omega_{cls}N^2 + \frac{\partial N}{\partial t}. \tag{41}$$

In this cases superposition of Eqs. (41), (29) and (30′) yields, instead of Eq. (35):

$$\frac{dN}{dt} = -4N^2\frac{\partial\overline{A}}{\partial t} - \omega_{cls}N^2, \tag{42}$$

which after substitution of Eqs. (30) and (31) takes the form

$$\frac{dN}{dt} = -N\beta\frac{3kT}{\gamma\varphi(\theta)}J_{dif}(t) - 36\pi^2\alpha D_s\Omega^{4/3}N^4, \quad \text{if } N\overline{A} = 0.5. \tag{43}$$

The source term $J_{dif}(t)$ should include also evaporation flux of chemically active elements (first of all Cs) from grain boundaries into bubbles, as explained in Section 4.2.

The model in the form of Eqs. (40) and (43), will be implemented in the MFPR code developed in collaboration between IBRAE (Moscow, Russia) and IRSN (Cadarache, France) for mechanistic modelling of fission product release from irradiated UO_2 fuel [3]. This will allow self-consistent calculation of bubbles growth and coalescence in the course of fission products generation and release in various regimes (including transients) and, in particular, a more adequate comparison of the model predictions with the above described measurements. This work is foreseen in the nearest future.

6. Conclusions

Two different mechanisms of grain face bubbles coalescence in irradiated UO_2 fuel proposed by Zacharie et al. [1] and White [5] are critically analysed and further developed. The first mechanism is based on consideration of random migration of bubbles over grain faces [1], whereas the second mechanism is based on consideration of growth and impingement of randomly distributed (immobile) face bubbles [5].

The coalescence of face bubbles due to their random migration is reconsidered on the base of the general kinetic theory [4]. This allows elimination of some inconsistencies in the modelling approach of [1] and improvement of the model predictions, especially in the case of continuous bubbles growth owing to absorption of gas atoms. The extension of the model to this case allows modelling of bubbles coalescence under irradiation conditions. In particular, it is shown that the migration mechanism can be effective for steady state irradiation conditions studied in the tests [9], however, is apparently insufficient for description of high-temperature annealing tests [1].

On the other hand, the improved mechanism of coalescence by growth and impingement of randomly distributed bubbles predicts rather weak decrease of face bubbles concentration under steady state irradiation conditions, however, becomes effective for simulation of high-temperature annealing tests with noticeable gas release. After attainment of the critical coverage, formation of channels on grain faces (interconnected with open porosity at grain edges) and their collapse owing to gas venting from face bubbles through the channels efficiently increase the bubble coalescence rate. In this case the bubble concentration variation is characterised by a rather strong (exponential) dependence on gas release and thus becomes significant under heat-up conditions of annealing or transient tests.

As a result, the general coalescence model which includes superposition of both mechanisms is formulated and proposed for implementation in the MFPR code [3], designed for mechanistic description of fission products release and fuel microstructure evolution; this will allow adequate modelling of grain face bubbles coalescence and fuel swelling under various operation conditions of nuclear reactors (steady irradiation, transient and post-irradiation annealing).

Acknowledgement

The author thanks Drs V. Ozrin and V. Tarasov (IBRAE, Moscow) for careful reading of the manuscript, valuable discussion and comments.

This work was supported by the Russian Foundation for Basic Research (RFBR) and by the International Science and Technology Center (ISTC), which are greatly acknowledged by the author.

References

[1] I. Zacharie, S. Lansiart, P. Combette, M. Trotabas, M. Coster, M. Groos, J. Nucl. Mater. 255 (1998) 85, 92–104.
[2] A.V. Berdyshev, M.S. Veshchunov, Modelling of Grain Face Diffusion Transport and Swelling in UO_2 Fuel, Preprint IBRAE-2002-14, Moscow, 2002.
[3] M.S. Veshchunov, V.D. Ozrin, V.E. Shestak, V.I. Tarasov, R. Dubourg, G. Nicaise, Nucl. Eng. Des. 236 (2006) 79.

[4] Ya.E. Geguzin, M.A. Krivoglaz, Migration of Macroscopic Precipitates in Solid Materials, Metallurgia, Moscow, 1971 (in Russian).
[5] R.J. White, J. Nucl. Mater. 325 (2004) 61.
[6] S. Chandrasekhar, Rev. Mod. Phys. 15 (1943) 1.
[7] L.K. Mansur, Nucl. Technol. 40 (1978) 5.
[8] L.K. Mansur, P.R. Okamoto, A. Taylor, Chey-Yu Li, in: R.J. Arsenault (Ed.), Int. Conf. Defects and Defect Clusters, BCC Metals and Their Alloys, August 14–16, 1973, Nucl. Metall. 18 (1973).
[9] S. Kashibe, K. Une, J. Nucl. Sci. Technol. 28 (1991) 1090.
[10] P.G. Shewmon, Trans. AIME 230 (1964) 1134.
[11] M.S. Veshchunov, J. Nucl. Mater. 346 (2005) 208.
[12] P.S. Maiya, J. Nucl. Mater. 40 (1971) 57.
[13] Hj. Matzke, in: L.C. Dufour, J. Novotny (Eds.), Surfaces and Interfaces of Ceramic Materials, Kluwer Academic, Dordrecht, 1989, p. 241.
[14] M.O. Marlowe, A.I. Kazanoff, J. Nucl. Mater. 25 (1968) 328.
[15] D.R. Olander, J. Nucl. Mater. 96 (1981) 243.
[16] S.Y. Zhou, D.R. Olander, Surf. Sci. 136 (1984) 82.
[17] C. Baker, J. Nucl. Mater. 71 (1977) 117.
[18] R.M. Cornell, G.H. Bannister, Proc. Brit. Ceram. Soc. 7 (1967) 855.
[19] M.E. Gulden, J. Nucl. Mater. 23 (1967) 30.
[20] E.Ya. Mikhlin, J. Nucl. Mater. 87 (1979) 405.
[21] R.J. White, M.O. Tucker, J. Nucl. Mater. 118 (1983) 1.
[22] T.J. Heames, D.A. Williams, N.E. Bixler, A.J. Grimley, C.J. Wheatley, N.A. Johns, P. Domogala, L.W Dickson, C.A. Alexander, I. Osborn-Lee, S. Zawadzki, J. Rest, A. Mason, R.Y. Lee, VICTORIA: A Mechanistic Model of Radionuclide Behaviour in the Reactor Coolant System under Severe Accident Conditions, NUREG/CR-5545, 1992.